npj | climate and atmospheric science

Article

Published in partnership with CECCR at King Abdulaziz University

https://doi.org/10.1038/s41612-024-00779-y

Pronounced spatial disparity of projected heatwave changes linked to heat domes and land-atmosphere coupling

Fenying Cai[1,2], Caihong Liu[3], Dieter Gerten[1,2], Song Yang[4,5], Tuantuan Zhang[4,5] ✉, Shuheng Lin[4] & Jürgen Kurths[1,6,7]

Heatwaves are projected to substantially increase at a global scale, exacerbating worldwide heat-related risks in the future. However, understanding future heterogeneous heatwave changes and their origins remains challenging. By analyzing the output of various climate models from the Coupled Model Intercomparison Project Phase 6, we found pronounced spatial disparity of projected heatwave increases in the Northern Hemisphere, even outstretching seven-fold inter-regional differences in extreme heatwave occurrences, attributed primarily to future changes in heat-dome-like circulations and soil moisture–temperature coupling. Specifically, we found that by the end of the 21st century, the modulations of combined Pacific El Niño and positive Pacific Meridional Mode on magnified heat-dome-like circulations would be translated into summertime hotspots over western Asia and western North America. Amplified soil moisture–temperature couplings then further aggravate the heatwave intensity over these two hotspots. This study provides support for formulating impact-based mitigation strategies and efficiently addressing the potential future risks of heatwaves.

Continuously increasing heatwave frequency and intensity over time at a global scale could bring about overwhelming social and economic consequences across continents[1–9]. While widespread increasing trends of the heatwave are detected in large parts of the Northern Hemisphere[10–14], a spatial disparity characterized by accelerated changes identified in hotspots and relatively weaker increases expressed as mitigated changes are also noticeable. Understanding this spatial disparity of heatwave changes and its origins, which is far from clear, can provide impact-based decision-making support for stakeholders. Hotspots, such as Europe[11–13] and western North America[15,16], have attracted an explosion of interest for the frequent record-breaking extreme heatwave events occurring in recent years. In addition to the relatively uniform warming associated with external forcing, the origins of hotspot centers were attributed to the changes in atmospheric circulations, including increasing persistent double jets[11], intensified Silk Road pattern teleconnections[12,13], and changing heat-dome-like circulations[15–17]. It was suggested that the accelerated heatwave trends over Western Europe are considerably bound up with more persistent double jets over Eurasia[11]. Heat domes, on the other hand, can explain half of the magnitude of the anomalous temperature over western North America in the summer of 2021[16]. This feature hints that atmospheric circulation may play considerable roles in the heterogeneity of the increase in heatwaves during the past several decades based on historical observations. Up to now, there has been a lack of unified investigation of the spatial heterogeneity in future projected heatwaves and their linkage to changing atmospheric circulations. In this study, we find that a pronounced disparity in extreme heatwave occurrences between different regions can outstretch 7-fold discrepancy (Fig. 2f), much more striking than those shown in commonly used metrics including heatwave cumulative intensity (Fig. 1a). This highlights the necessity to disentangle the origins of the spatial pattern in projected heatwave intensifications, in particular for the potential influences of future changes in atmospheric circulations, oceanic temperature, and land-atmosphere coupling.

Oceanic warming/cooling can significantly modulate atmospheric teleconnections via triggering/suppressing convection activity and hence is a crucial driver of global heatwave variability[18,19]. El Niño–Southern Oscillation (ENSO), as the dominant mode of tropical Pacific sea surface

[1]Potsdam Institute for Climate Impact Research (PIK), Member of the Leibniz Association, P.O. Box 60 12 03 D-14412 Potsdam, Germany. [2]Department of Geography, Humboldt-Universität zu Berlin, 10099 Berlin, Germany. [3]Department of Water and Climate Risk, Institute for Environmental Studies, Vrije University Amsterdam, 1087HV Amsterdam, Netherlands. [4]School of Atmospheric Sciences, Sun Yat-sen University and Southern Marine Science and Engineering Guangdong Laboratory (Zhuhai), 519082 Zhuhai, China. [5]Guangdong Province Key Laboratory for Climate Change and Natural Disaster Studies, Sun Yat-sen University, 519082 Zhuhai, China. [6]Department of Physics, Humboldt-Universität zu Berlin, 10099 Berlin, Germany. [7]School of Mathematical Sciences, SCMS, and CCSB, Fudan University, 200433, Shanghai, China. ✉e-mail: zhangtt75@mail.sysu.edu.cn

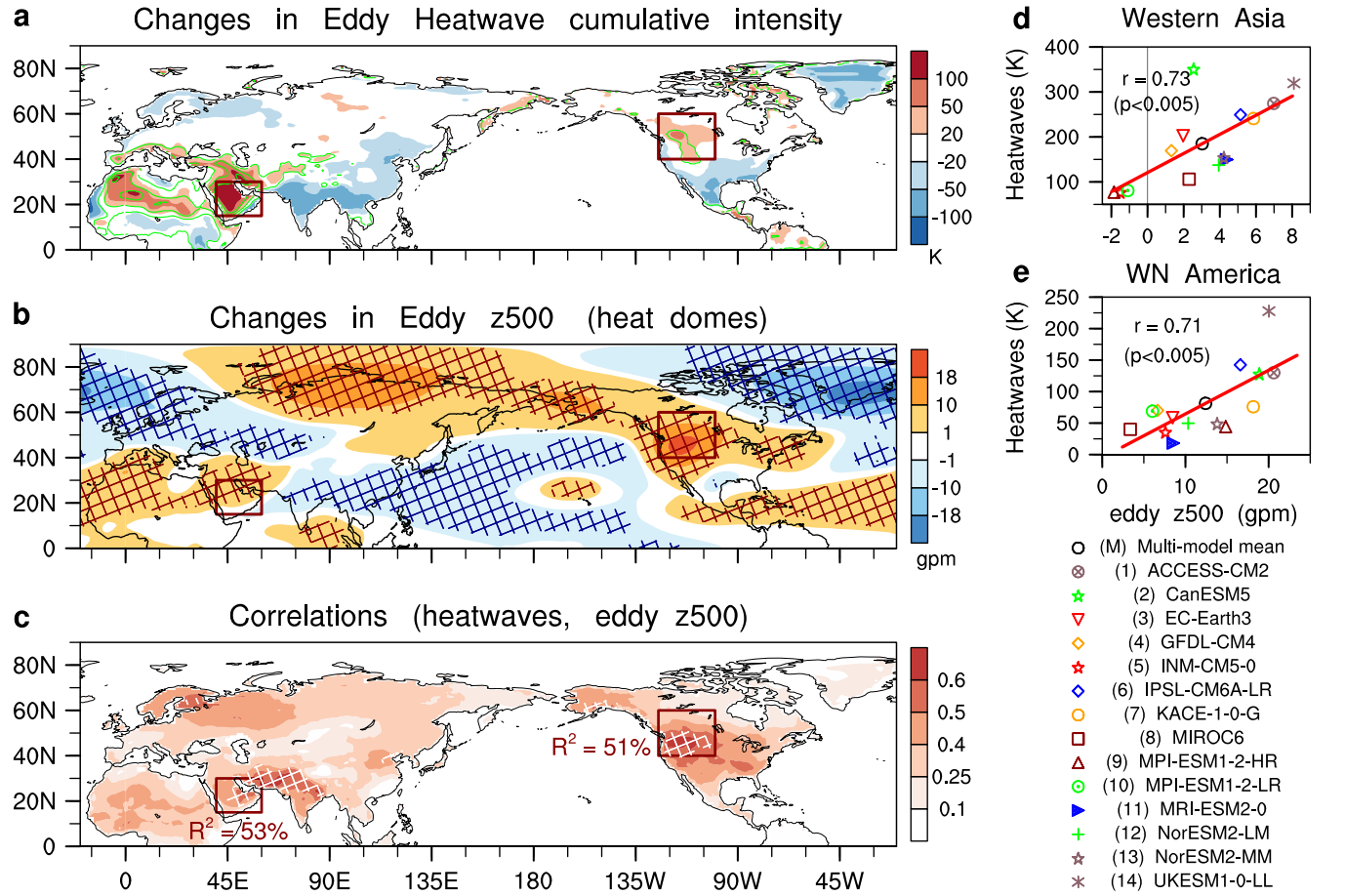

Fig. 1 | Multi-model mean of long-term future summertime heatwave and eddy z500 changes in the Northern Hemisphere under the SSP585 scenario. Future changes are calculated as the averaged difference between 2071–2100 under the SSP585 scenario and the reference period 1991–2020 (combined historical simulation and SSP585 scenario) for **a** eddy heatwave cumulative intensity (eddy HWI identified as HWI being removed zonal mean; shadings; units: K), HWI (green contours shown at 100, 150, and 200 K) and **b** eddy z500 (geopotential height at 500 hPa being removed zonal mean; units: gpm). Hatched areas in **b** show where at least 11 models (>78% of the total 14 models) project the eddy z500 changes with same signs. **c** Correlation coefficient between projected HWI and eddy z500 changes in 420 summers during 2071–2100 by 14 models. Hatched areas in **c** show where the inter-model correlation coefficient between projected HWI changes and eddy z500 changes (2071–2100 average minus 1991–2020 average) exceeds the 95% confidence level. Future HWI changes (units: K) versus eddy z500 changes (units: gpm) for **d** western Asia and **e** western North America. The red boxes in **a**–**c** present the domain of western Asia (15°–30°N, 40°–60°E) and western North America (40°–60°N, 125°–100°W). The inter-model explained variances (R^2) between heatwave changes and eddy z500 changes for western Asia and western North America are also shown in (**c**). The labels denoting the 14 models are shown in the bottom right corner.

temperature (SST) variability, could modulate heatwave variations over Europe[20], North America[21], East Asia[22], South Asia[23], and Australia[24,25]. In addition, the European heatwaves in 2003[26] and 2015[27] were thought to be driven by SST anomalies in the Indian Ocean and the North Atlantic, respectively. The Pacific SST anomaly identified as the Pacific Extreme Pattern as a precursor was observed even 50 days in advance of the occurrences of hot days over the eastern United States[28]. Those oceanic signals are projected to change remarkably in the future, but their potential influences on the nonuniform heatwave trends have received little attention by far.

The impacts of atmospheric circulations on heatwaves can be further modulated by the in situ soil moisture–temperature coupling, which has been emphasized increasingly in recent studies[29–36]. By altering the surface latent heat flux and thereafter reducing the evaporative cooling, soil moisture deficits could promote the occurrences of extreme local heat, especially in the mid-latitudes[29–32]. For example, the hot extreme over western North America in 2021 was amplified by a soil moisture deficit, which can enhance the intensity and prolong the duration of heat-dome-like circulations[16]. In future projections, intensified soil moisture–temperature feedback will additionally increase the likelihood of extremely high temperature[35,36]. It is certainly to suppose that together with atmospheric circulations, land–atmosphere feedback will provide insights for heterogeneous changes in heatwaves.

In this study, future changes with accelerated and mitigated areas for heatwave and their linkage to heat-dome-like circulation changes are investigated based on the output of various climate models from the Coupled Model Intercomparison Project Phase 6 (CMIP6)[37]. The amplified risks of climate model-projected hotspots, compared with other regions in the same latitudes, by heat-dome-like circulation changes, are quantified. Furthermore, the roles of tropical asymmetric SST in heat-dome-like circulation changes and additional effects of land–atmosphere coupling trends on the nonuniform spatial pattern of projected heatwave intensifications are identified.

Results

Connection between projected future changes in heatwaves and heat-dome-like circulations

Before examining the future changes projected by CMIP6 climate models, we evaluate the models' performance in simulating historical features of heatwaves. The outputs of 14 CMIP6 models are validated with respect to their fidelity in simulating heatwave cumulative intensity (HWI), which is identified as summertime accumulated margins of T_{max} exceeding the 90th

percentile (see the "Methods" for details). By comparing the probability density function (PDF) of HWI in the ERA5 reanalysis dataset[38] and that in the historical simulations by 14 CMIP6 models for the period 1950–2014, we find that the models can indeed basically reproduce the observed PDF in HWI, although the multi-model mean of the 14 models slightly underestimates the frequency of high-HWI events (see Supplementary Fig. S1). With pattern correlation significant at a 99% confidence level, the multi-model mean could basically simulate the spatial pattern of ERA5 HWI trends in 1950–2014 (see Supplementary Fig. S2). In particular, the historical hotspot over Eastern Europe can be well reproduced in the multi-model mean and most of the models (see Supplementary Figs. S2, S3).

Taking advantage of the models' reasonable performance, the projected future changes in heatwave by the multi-model average of the 14 CMIP6 models are examined. Contrasts in HWI between the long-term future (2071–2100) under the SSP585 scenario and the reference period (1991–2020; combined historical simulation and SSP585 scenario) are displayed in Fig. 1a. Pronounced spatial disparity of the projected changes in heatwave intensity is exhibited, although heatwave intensity generally increases (Fig. 1a). An accelerated increase in heatwave intensity is presented by the multi-model mean and most of the 14 CMIP6 models over the Mediterranean, western Asia, and western North America (Fig. 1a, see Supplementary Fig. S4). We identify western Asia and western North America as the hotspots over the subtropics and the mid-latitudes in the long-term future, respectively. In contrast, relatively weaker changes are projected over northern Europe, South Asia, East Asia, and Greenland (Fig. 1a, see Supplementary Fig. S4). The spatial pattern of HWI changes is similar to which of summertime surface temperature change (Fig. 1a, see Supplementary Fig. S5). For the two hotspots, highly inter-model correlation coefficients up to 0.9 are observed between projected HWI trends and surface temperature changes (see Supplementary Fig. S6a, d), since increasing in mean temperature could exacerbate the cumulative intensity of extreme heatwaves.

Such a spatial disparity of projected heatwave intensifications seems to be closely linked to the future changes in heat-dome-like circulation depicted by zonally asymmetric geopotential height at 500 hPa[16] (eddy z500; see the "Methods" section for details). An accelerated heatwave increase coincides with intensified heat-dome-like circulations, while mitigated heatwave changes coincide with weakened eddy z500 (Fig. 1a, b, see Supplementary Figs. S4, S7). Across all land regions in the Northern Hemisphere, projected heatwave intensifications are significantly correlated with the changes in eddy z500 in a total of 420 months in the long-term future by all 14 CMIP6 models (Fig. 1c), possibly due to a well-recognized hydrostatic balance relationship that thickness between pressure levels is proportional to layer mean temperature. In particular, the 2071–2100 averaged HWI changes are found to be highly dependent on eddy z500 changes for the two hotspots (Fig. 1d, e), because 53% (51%) of the inter-model variances in HWI changes over western Asia (western North America) are explained by eddy z500 changes. Significant relationships between summer-mean eddy z500 and cumulative intensity of extreme heatwaves are mediated by summer-mean surface temperature (see Supplementary Fig. S6a, b, d, e). The close linkage between surface warming and middle-upper tropospheric anticyclones is consistent with the hydrostatic relationship. These results suggest that the heat-dome-like circulation changes are significantly linked to the heatwave accelerations over western Asia and western North America. Similar features can be obtained by the projection under the SSP245 scenario, although with a relatively weaker magnitude (see Supplementary Fig. S8). It is noteworthy that the inter-model dependence between simulated HWI and eddy z500 over the two hot spots are significant for the long-term future (2071–2100), but not significant for the mid-term future (2036–2065) as shown in Supplementary Fig. S9. Accelerated heatwave changes are also discovered over western Asia and western North America as depicted by other heatwave metrics, including heatwave cumulative frequency and heatwave averaged intensity, under both SSP585 and SSP245 scenarios (see Supplementary Figs. 10, 11).

Future climate change includes (i) a spatially uniform component, known as thermodynamic change and (ii) a zonally asymmetric component caused by dynamic change[10,11]. The first component may be interpreted as global uniform warming, which is accompanied by a homogeneous HWI increase and a geopotential height rising globally (Fig. 2a versus c). In contrast, intensified eddy z500, probably induced by atmospheric teleconnection alterations, is characterized by a magnified gradient between relatively high- and low-pressure centers which facilitates the spatial disparity (the second component) (Fig. 2a versus b). Here, western Asian accelerated warming is used to further epitomize the roles of global uniform warming and intensified heat-dome-like circulations. We analyze the daily distribution of near-surface temperature maximum (T_{max}) over the subtropics during the reference period (1991–2020), the mid-term future (2036–2065), and the long-term future (2071–2100). Global uniform warming is dominant over all regions because the PDF of T_{max} over each place shifts towards a high-temperature state from the beginning to the end of the 21st century, which remarkably increases the probability of record-shattering heatwaves (Fig. 2d, see Supplementary Fig. S12a–e). Given the well-recognized global uniform warming, we focus on the connection between the projected changes in heat-dome-like circulations and related heterogeneous HWI in this study. A marked disparity between the frequencies of heat extremes over western Asia and other places in the subtropics is projected. In particular, the likelihood of extreme heat days (>5.5 std above the historical conditions) over western Asia (10.3%) could become three times as high as that over the other subtropical land areas (3.9%), and even nearly seven times as high as that over South Asia (1.5%) by the end of the century under the SSP585 scenario (Fig. 2e, f, see Supplementary Figs. S12, 13). In addition to increases in mean temperature, accelerated HWI increases over western Asia are also attributed to increases in the variances of T_{max}. In particular, extreme temperature increases faster compared with the mean temperature changes, especially over western Asia, by an amplified ratio of ~18% (see Supplementary Fig. S14). This spatial disparity in extreme heatwave occurrences, closely connected to heat-related risks, is more pronounced than that shown in heatwave cumulative intensity or averaged intensity (Fig. 1a, see Supplementary Fig. S10b). It is necessary to identify the patterns as well as the origins of the extreme heatwave risks with significant spatial variations. Similar amplified occurrences of extreme heat days are also projected over western North America compared with the other mid-latitude land areas, although the spatial difference is much weaker over the mid-latitudes compared with the subtropics (see Supplementary Fig. S12d–f).

Roles of tropical asymmetric changes in sea surface temperature

Heat-dome-like circulations are generally embedded in global climate teleconnections, which are manifested by internal variability or modulated eminently by convective activity associated with the tropical sea surface temperature (SST) anomaly[18,19]. A strong consensus is projected by most of the CMIP6 models, indicating that SST increases exceptionally faster over the tropical and subtropical central-eastern Pacific (Fig. 3a), probably linked to more frequent concurrences of El Niño events and a positive phase of the Pacific Meridional Mode (PMM+)[39,40]. We define a tropical Pacific asymmetric SST index as the areal-averaged zonally asymmetric SST (eddy SST) over the Northern Hemisphere tropical central-eastern Pacific (boxes in Fig. 3a, b; see the "Methods" section for details). The inter-model regressions of eddy SST change onto the tropical Pacific asymmetric SST index clearly indicate that the asymmetric SST changes over the tropical eastern Pacific are negatively linked to eddy SST changes near the Maritime Continent and over the Northern Hemisphere subtropical Atlantic, rather than being isolated (Fig. 3b). The models show stronger El Niño and PMM+ patterns in the long-term future tends to project stronger convection and below-average eddy z500 over the tropical central-eastern Pacific, and vice versa (Fig. 3c). Notably, intensified heat-dome-like circulations are projected over western Asia and western North America as a consequence of the increased convective activity over central-eastern Pacific (Fig. 3c). In addition,

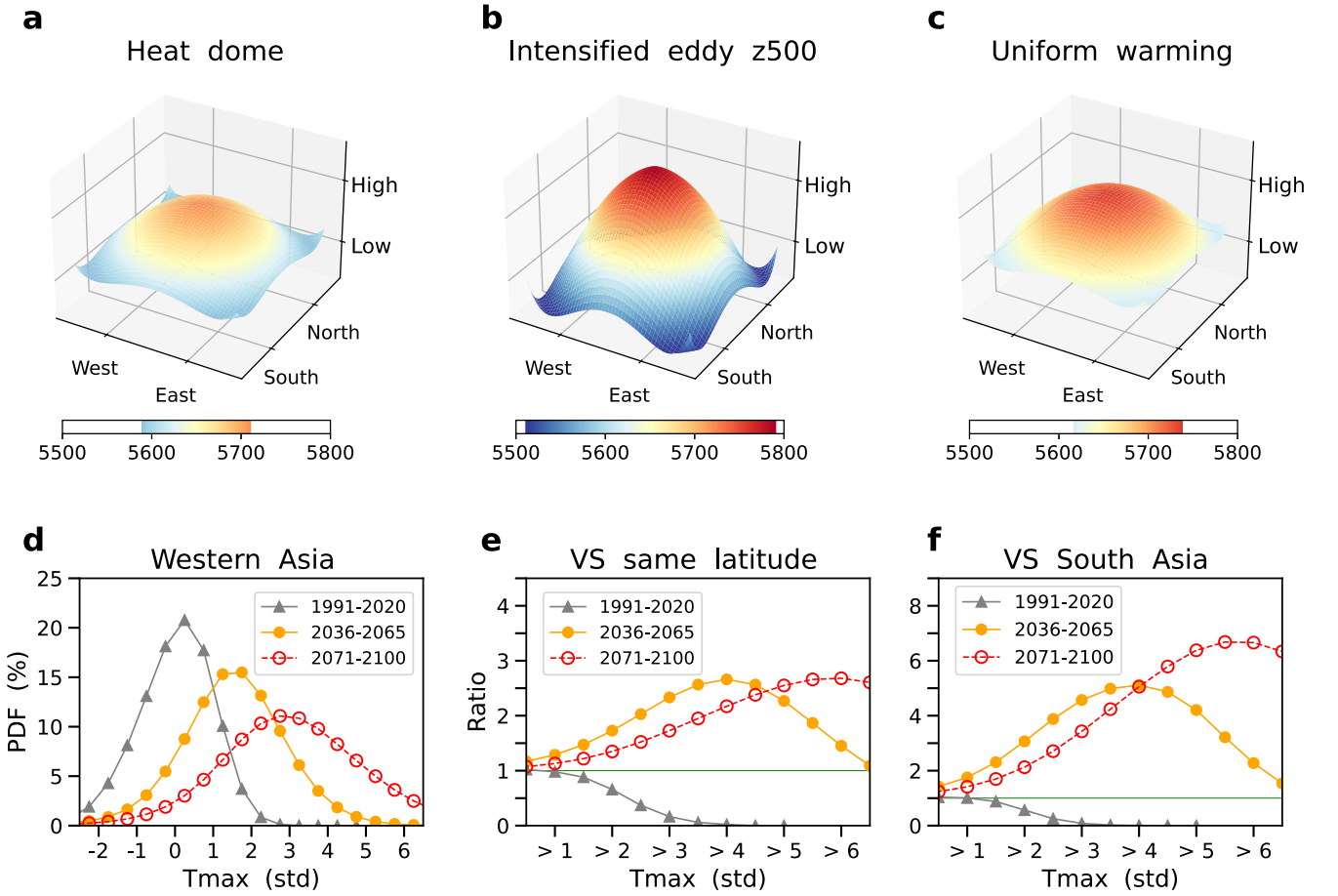

Fig. 2 | Accelerated increase in heatwave intensity over western Asia associated with intensified eddy z500 under the future SSP585 scenario. Schematic diagram of **a** heat-dome-like circulation and its future change depicted by **b** intensified eddy z500 and **c** global uniform warming. **d** Probability density functions (PDF) of T_{max} over western Asia (15°–30°N, 40°–60°E) for the period 1991–2020 in combined historical simulation and SSP585 scenario (gray line with triangles), and 2036–2065 (orange line with solid circles) and 2071–2100 (red line with hollow circles) under the SSP585 scenario. The ratio of accumulated PDF in T_{max} over western Asia versus that over **e** subtropical region (15°–30°N) excluding western Asia, and versus that over **f** South Asia (15°–30°N, 70°–85°E). T_{max} is normalized by subtracting the mean value and then dividing by the standard deviations of values during the period 1991–2020 in combined historical simulation and SSP585 scenario before calculating the PDF.

weakened heat-dome-like circulations as well as mitigated HWI changes are found over Greenland as a response to the Rossby wave train related to El Niño and PMM+ patterns[41] (Figs. 1a, b and 3c).

In addition to inter-model correlations, the amplified teleconnections related to El Niño and PMM+ are validated by comparing the quantitative occurrences of ocean-atmosphere coupling events among the 14 models. At least 11 (>78%) of all 14 models show an increase or remain unchanged in the frequencies of both El Niño summers and combined El Niño and PMM+ summers (Fig. 3d, e), in agreement with previous studies[39,40,42,43]. A high inter-model consensus is projected by the models because only three models simulated a decrease in both El Niño summers concurrent with PMM+ or not (Fig. 3d, e). Correspondingly, intensified heat-dome-like circulations are detected over western Asia during El Niño summers (Fig. 3f, see Supplementary Fig. S15), while an intensified eddy z500 is identified over western North America during combined El Niño and PMM+ summers (Fig. 3g). The increasing frequency of El Niño summers gives rise to more large-scale heat-dome-like circulations over western Asia and the Arabian Sea through the west-east shift of the tropical Walker circulations[44], featured as zonal eddy z500 dipole and upper-level stream function dipole over the Pacific and Indian Oceans (Fig. 3f, see Supplementary Figs. S15, 16). On the other side, the poleward-propagating atmospheric Rossby wave train known as Pacific-North American pattern, as a response to El Niño and PMM+, boosts the intensified occurrences of heat-dome-like circulations over western North America (Fig. 3g). The changing atmospheric teleconnections, including zonal Walker circulations and poleward atmospheric wave trains, bridge the tropical Pacific asymmetric SST changes and eddy z500 intensifications over the two hotspots. Therefore, the tropical Pacific asymmetric SST index and two-hotspot eddy z500 changes are highly correlated among models ($p < 0.005$; Fig. 3h, i). Reasonably, the HWI changes over western Asia and western North America projected by a climate model significantly rely on the simulated tropical Pacific asymmetric SST changes ($p < 0.05$; Fig. 3j, k).

Roles of changes in soil moisture–temperature coupling

The spatial disparity of future changes in heatwave can be roughly sketched by heat-dome-like circulation changes, but some details seem to be overlooked. For example, the strongest eddy z500 changes are projected over western North America, much higher compared with western Asia, but relatively weaker heatwave accelerations are projected over western North America than that over western Asia (Fig. 1). It seems that only the circulation change may be not sufficient to explain the exceptional strongest increase in heatwave intensity over western Asia. In general, local land–atmosphere couplings can modulate the relationship between heatwave and heat-dome-like circulations by changing the surface evaporative cooling[29–31], which may play a role in the disproportionate relationship between heatwave and heat-dome-like circulations. The future changes in the strengths of soil moisture–temperature couplings are examined in the following.

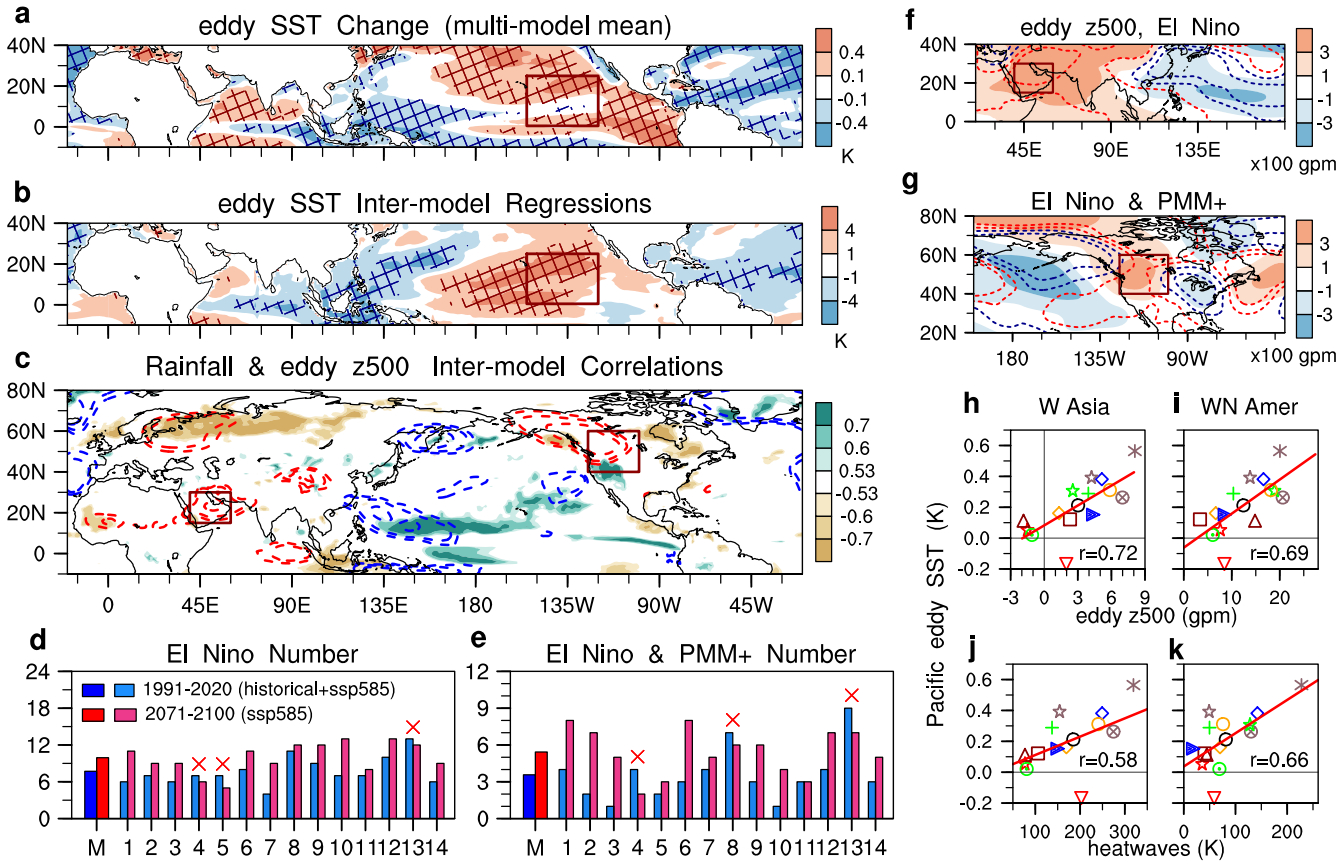

Fig. 3 | Impacts of El Niño and positive phase of the Pacific Meridional Mode (PMM+) on the projected changes in eddy z500 under the future SSP585 scenario. **a** Multi-model mean of the changes in zonally asymmetric sea surface temperature (eddy SST; shadings; units: K) between 2071–2100 and 1991–2020, and hatched areas show where at least 11 models (>78%) project the same signs. **b** Inter-model regression coefficients of eddy SST changes onto tropical Pacific asymmetric SST changes (0°–25°N, 155°–120°W, red box in (**a**–**b**); see the "Methods" section for details), and hatched areas show where $p < 0.05$. **c** Inter-model correlation coefficients of precipitation changes (shadings; $p < 0.05$) and eddy z500 changes (red contours shown at 0.53, 0.6, and 0.7, and blue contours shown at −0.53, −0.6, and −0.7) onto tropical Pacific asymmetric SST changes. Number of **d** El Niño summers and **e** those El Niño summers with PMM+ during the period 1991–2020 (blue bars) and the period 2071–2100 (red bars) by multi-model mean (*M*) and 14 individual models. The models that show a decrease are indicated by red cross markers in (**d**) and (**e**). Accumulated eddy z500 anomalies (shadings; units: 10^2 gpm) for **f** El Niño summers, and **g** the El Niño summers with PMM+ during the period 2071–2100. The differences in accumulated eddy z500 anomalies (red contours shown at 0.5 and 1.5; blue contours shown at −0.5 and −1.5; units: 10^2 gpm) between 2071–2100 and 1991–2020 are also shown in (**f**) and (**g**), respectively. Projected tropical asymmetric SST changes (units: K) versus **h** and **i** eddy z500 changes (units: gpm), and **j** and **k** heatwave cumulative intensity (units: K). **h** and **j** are for western Asia, and **i** and **k** are for western North America. The results in 1991–2020 are obtained from combined historical simulations and the SSP585 scenario, while those in 2071–2100 are from the SSP585 scenario. The red boxes in **c**, **f**, **g** present the domain of western Asia (15°–30°N, 40°–60°E) and western North America (40°–60°N, 125°–100°W).

We investigate the dependence between near-surface maximum temperature (T_{max}) and soil moisture based on their Pearson correlations at daily time scales. The negative correlations between T_{max} and soil moisture are enhanced over most of the land areas in the Northern Hemisphere projected by the multi-model median of the 14 CMIP6 models (Fig. 4a, see Supplementary Fig. S17), which is consistent with previous findings indicating that soil moisture–atmosphere coupling accelerates global warming[35,36]. The multi-model median of correlation coefficients is adopted as multi-model estimate to minimize the spurious effects from the outlier with unusually high or low correlation coefficients. In particular, the intensification of land–atmosphere couplings reaches the strongest over western Asia, much higher than that over western North America (Fig. 4a, see Supplementary Fig. S17), explaining why heatwave is projected to be more exacerbated over western Asia compared with western North America and other areas (Fig. 1a). Amplifications of the negative correlations between surface temperature and soil moisture over western Asia are projected by all 14 models (Fig. 4b, see Supplementary Fig. S17), demonstrating a very high inter-model agreement. For the Asian monsoon region with weakened heat-dome-like circulations, intensified soil moisture–temperature correlations over East Asia favor a relatively larger HWI increase compared with the mitigated HWI increase and attenuated land–atmosphere coupling over South Asia (Figs. 1, 4a, see Supplementary Fig. S17).

Considering that soil moisture changes can feed back onto large-scale atmospheric heat-dome-like circulation[45–49], the changes in the relationships between eddy z500 and soil moisture, as well as eddy z500 and T_{max} tendency at daily time scales are also examined (Fig. 4c, d, see Supplementary Figs. S18, S19). For western Asia, most models (at least 12 models, >85%) project an amplified inverse correlation between eddy z500 and soil moisture (Fig. 4c, see Supplementary Fig. S18), and an intensified positive dependence between eddy z500 and T_{max} tendency (Fig. 4d, see Supplementary Fig. S19). Magnified feedback among eddy z500, soil moisture, and T_{max} facilitated the establishment of the most accelerated heatwave increase over western Asia compared with other regions around the world. In contrast, weakened couplings of eddy z500-soil moisture and eddy z500-T_{max} tendency are projected over western North America (Supplementary Figs. S18, S19), explaining why heatwave acceleration over western North

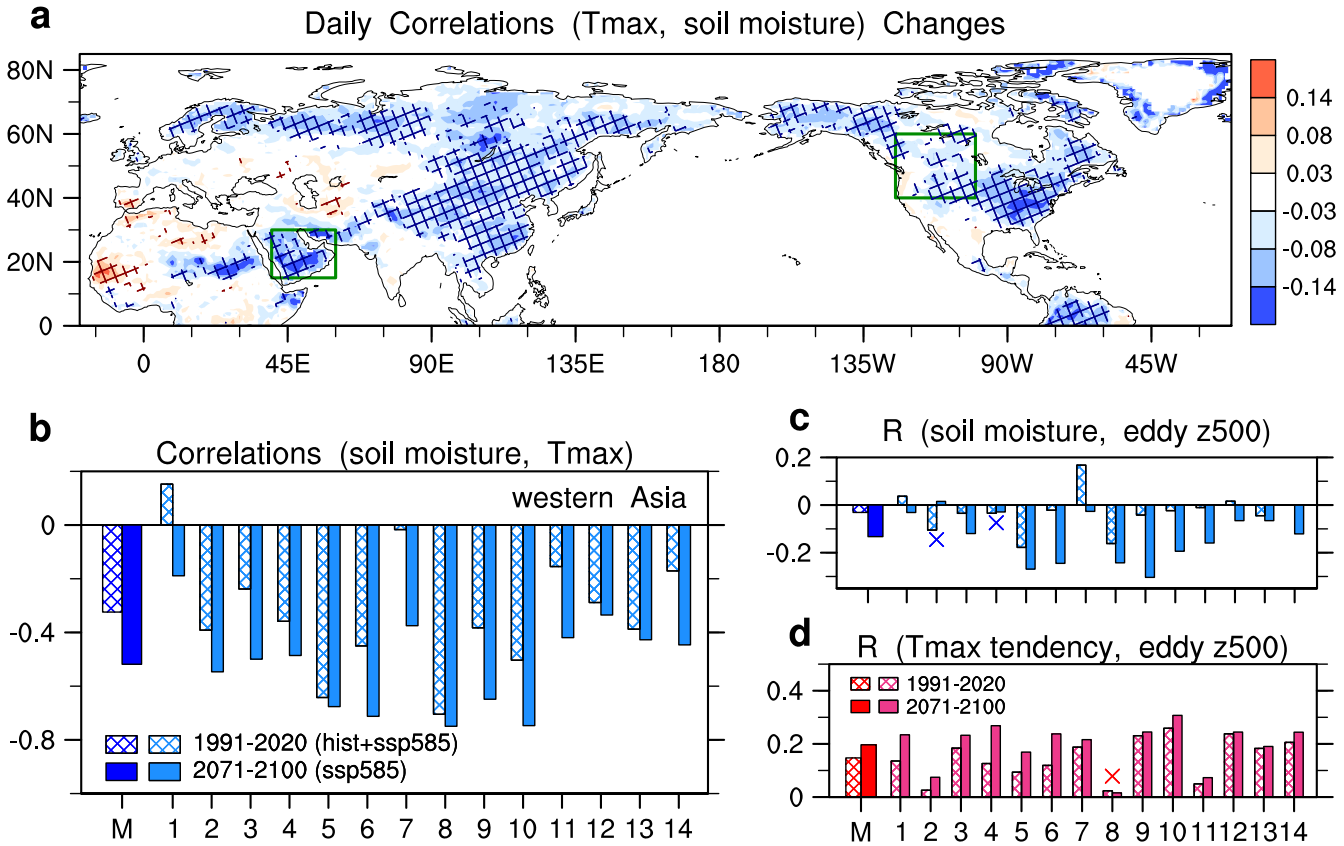

Fig. 4 | Amplified temperature–soil moisture-eddy z500 feedback over western Asia under the future SSP585 scenario. a Spatial distribution of multi-model estimated changes from reference simulation (1991–2020) to SSP585 scenario (2071–2100) for the correlation coefficients between daily T_{max} and soil moisture. The multi-model estimate of correlation change is the median value in the results of 14 CMIP6 models. Hatched areas in **a** show where at least 11 models (>78% of the total 14 models) project the correlation changes with the same signs. Correlation coefficients at daily time scales for western Asia between **b** T_{max} and soil moisture, **c** soil moisture and eddy z500, and **d** T_{max} tendency and eddy z500 for the period 1991–2020 in combined historical simulation and SSP585 scenario (hatched bars) and for the period 2071–2100 under the SSP585 scenario (filled bars) by multi-model median (*M*) and 14 CMIP6 models. Models showing an opposite change with multi-model median are indicated by colored cross markers in (**b**–**d**).

America is not as strong as that over western Asia, even though the most intensified heat-dome-like circulation changes are projected over western North America (Fig. 1a, b). Based on a linear regression model, we exhibit that nearly equal contributions (~35%) to the western Asian HWI changes are estimated from the changes in soil moisture–temperature couplings and eddy z500 (see Supplementary Fig. S20). In contrast, for western North American HWI changes, the contributions of eddy z500 changes (106%) are dominant compared with the changes in soil moisture–temperature couplings (8%). It is emphasized that intensified land–atmosphere couplings play an important role in the most accelerated HWI changes over western Asia, compared with those over western North America and other regions in the Northern Hemisphere.

Discussion

In this study, the spatial heterogeneity of future heatwave intensity changes and its origins are examined by comparing the output of future projections (2071–2100) under the SSP585 and SSP245 scenarios, and historical simulations (1991–2020). We find that pronounced spatial disparity in heatwave changes by the end of the 21st century is projected being in agreement by most of the 14 CMIP6 models. It is highlighted that western Asia and western North America are projected as summertime hotspots in the Northern Hemisphere, closely connected to intensified heat-dome-like circulations. The likelihood of extreme heat day (>5.5 std) over western Asia could reach three times as high as over other subtropical land area and even seven times as high as that over South Asia. The disparity in extreme heatwave occurrences between various regions is much higher than that expected from the spatial differences in heatwave cumulative intensity changes, highlighting the necessity to disentangle the responsible physical mechanisms. It is noteworthy that the obvious shift of hot spots from eastern Europe for historical periods to projected accelerated HWI trends over western Asia and western North America, which provide insights for formulating impact-based mitigation strategies and efficiently addressing the potential future risks of climate extremes.

To identify the origins of regional contrasts in heatwave changes, the influences of tropical asymmetric SST changes and land–atmosphere coupling shifts are further examined. We discover that the two intensified heat-dome centers (western Asia and western North America) are facilitated by remote El Niño-like and PMM + SST changes over the tropical Pacific, both of which can modulate the strengths of heat-dome-like circulations over the two hotspots. Meanwhile, the local amplified surface soil moisture–temperature couplings favor the heatwave accelerations over western Asia and western North America. Particularly, the strongest warming over western Asia is largely linked to the most magnified land–atmosphere feedback over the Arabian Peninsula. Overall, the spatial disparity of projected heatwave intensifications is generally sketched by the changes in heat-dome-like circulations linked to increasing El Niño and PMM+ events and amplified local land–atmosphere feedback. The quantification and attribution of future spatially nonuniform warming in this study support addressing future climate extreme risks according to regional distinctions.

Although the spatial disparity of future heatwave increases and its origins are revealed by the projected changes in agreement and correlation

analysis among CMIP6 models for heatwave intensity, eddy z500, and SST in the current study, the underlying physical explanations of the found patterns need to be corroborated by further studies using advanced statistical techniques such as casual discovery methods[50]. The interpretation regarding the relationship between the changes in the central-eastern Pacific SST and heat domes in the future projection may have some uncertainties due to the model's imperfect performance. In addition, the potential impacts of heterogeneity in heatwave changes on society and economics remain to be discussed. During recent decades, social and economic risks caused by heat extremes have attracted high concerns for their widespread implications and need to be quantified in term of further socioeconomic research. Another future task is the risks associated with the spatial changes in compound extremes[51–55], including heat–dry[52,53] and heat–humid[54,55] extremes, given their exacerbated impacts compared with the univariate extremes. A thorough investigation of the spatial distinctions in future projections of compound extreme events is conducive to addressing the potential risks precisely.

Methods

Datasets

The atmospheric variables derived from the European Centre for Medium-range Weather Forecasts Reanalysis v5 (ERA5) datasets[38] with a horizontal resolution of 1° × 1°, are analyzed in this study. Daily T_{max} is derived from the maximum hourly 2-m air temperature ($T_{2\,m}$) in each day. Model outputs of daily T_{max}, 500-hPa geopotential height ($H500$), soil moisture, monthly $H500$, sea surface temperature (SST), and precipitation from the CMIP6 historical simulations[37] during 1950–2014 and the SSP585 and SSP245 scenarios during 2015–2100 are also examined. Future changes relative to the reference period 1991–2020 will be investigated in this study. For future changes under the SSP585 (SSP245) scenario, the historical climatology is a combination of the historical simulation 1991–2014 and the SSP585 (SSP245) scenario 2015–2020. The output of each model simulation is interpolated into 1° × 1° before analysis. Fourteen CMIP6 models with output of aforementioned daily and monthly variables are included: ACCESS-CM2, CanESM5, EC-Earth3, GFDL-CM4, INM-CM5-0, IPSL-CM6A-LR, KACE-1-0-G, MIROC6, MPI-ESM1-2-HR, MPI-ESM1-2-LR, MRI-ESM2-0, NorESM2-LM, NorESM2-MM, and UKESM1-0-LL (see Supplementary Table 1).

Intensities of heatwaves and heat-dome-like circulations

For the future projection in the mid-term future (2036–2065) and long-term future (2071–2100), heatwaves are identified over land grids when daily T_{max} exceeds its 99th percentile threshold (θ_{99th}) of the reference period of 1991–2020 for at least 3 consecutive days[11,56,57]. The θ_{99th} for a specific day is derived from a total of 30 years × 15 days (7 days on either side of the target day). For instance, the threshold value on 21 July is equivalent to the 99th percentile of T_{max} on 14–28 July during 1991–2020. Heatwave cumulative intensity (HWI) is defined as the accumulated values $\sum(T_{max} - \theta_{99th})$ for all heatwave events in each summer. Heatwave averaged intensity is equal to HWI divided by the number of heatwave days. The main conclusions in this study remain unchanged if future projected heatwaves are identified based on the 90th percentile threshold of the reference period 1991–2020. In addition, for the historical period 1950–2014, heatwaves are identified based on the 90th percentile threshold of the period 1991–2020, because the 90th percentile threshold is commonly used for the observed heatwaves in previous studies[11,55,56]. Deviations of geopotential height at 500 hPa from the zonal mean (eddy Z500) are adopted to indicate the intensity of atmospheric heat-dome-like circulations[16].

El Niño summer and positive phase of Pacific Meridional Mode (PMM+)

When June–July–August (JJA) averaged sea surface temperature anomaly (SSTA) over the Niño 3.4 region (5°S–5°N, 170°–120°W) exceeds 0.5 K, an El Niño summer is recognized. To compare the zonally asymmetric pattern of SST between historical simulations and future projections, SSTA is defined as the SST anomaly deviated from the period 2071–2100 for the long-term future projections and deviated from the period 1991–2020 for the reference period. A positive phase of the Pacific Meridional Mode (PMM+) is identified when JJA-mean SSTA over the tropical eastern North Pacific (15°–25°N, 150°–120°W)[58] exceeds 0.3 K.

To investigate the influences of SST changes featured as more El Niño and PMM+ events in the future, we define a tropical Pacific asymmetric SST index as the areal-averaged zonally asymmetric SST changes in the tropical eastern Pacific (0°–25°N, 155°–120°W). The domain of tropical eastern Pacific is shown by the red boxes in Fig. 3a, b. Zonally asymmetric SST (also named eddy SST) change is identified as the SST change deviation from its zonal mean.

Couplings among T, soil moisture, and eddy z500

Future changes in land–atmosphere couplings are investigated by comparing the correlation coefficients between T_{max} and soil moisture at daily time scale for the period 1991–2020 (combined historical simulations and SSP585 scenario) and the period 2071–2100 in the long-term future projections. To consider the role of heat-dome-like circulations, the correlations between eddy z500 and T_{max} tendency, and between eddy z500 and soil moisture are also examined at a daily time scale. The climatological seasonal cycle and temporal linear trends in the daily anomaly of T_{max}, soil moisture, and eddy z500 are removed before further correlation analysis. To measure the synoptic variation, T_{max} on each day (D0) is calculated as the difference between one day after (D0 +1 day) and one day before (D0 −1 day):

$$T_{max}\text{tendency(D0)} = T_{max}\,(\text{D0} + 1\text{day}) - T_{max}\,(\text{D0} - 1\text{day})$$

T_{max} tendency on 1 June and 31 August are excluded, because one of their adjacent dates (31 May or 1 September) does not belong to JJA.

Data availability

All data needed to evaluate the conclusions are presented in the article. The ERA5 single-level and multi-level variables are available at https://doi.org/10.24381/cds.adbb2d47 and https://doi.org/10.24381/cds.bd0915c6, respectively. The outputs of CMIP6 simulations are available at https://esgf-node.llnl.gov/search/cmip6/.

Code availability

The codes used to generate the results of this study are available on request from the authors.

Received: 28 March 2024; Accepted: 18 September 2024;
Published online: 30 September 2024

References

1. Coumou, D. & Rahmstorf, S. A decade of weather extremes. *Nat. Clim. Chang.* **2**, 491–496 (2012).
2. Coumou, D. & Robinson, A. Historic and future increase in the global land area affected by monthly heat extremes. *Environ. Res. Lett.* **8**, 034018 (2013).
3. Christidis, N., Jones, G. S. & Stott, P. A. Dramatically increasing chance of extremely hot summers since the 2003 European heatwave. *Nat. Clim. Chang.* **5**, 46–50 (2015).
4. Mazdiyasni, O. & AghaKouchak, A. Substantial increase in concurrent droughts and heatwaves in the United States. *Proc. Natl Acad. Sci. USA* **112**, 11484–11489 (2015).
5. Meehl, G. A. & Tebaldi, C. More intense, more frequent, and longer lasting heat waves in the 21st century. *Science* **305**, 994–997 (2004).
6. Perkins-Kirkpatrick, S. E. & Lewis, S. C. Increasing trends in regional heatwaves. *Nat. Commun.* **11**, 3357 (2020).
7. Perkins, S. E., Alexander, L. V. & Nairn, J. R. Increasing frequency, intensity and duration of observed global heatwaves and warm spells. *Geophys. Res. Lett.* **39**, 20 (2012).

8. Sun, Y. et al. Rapid increase in the risk of extreme summer heat in Eastern China. *Nat. Clim. Chang.* **4**, 1082–1085 (2014).
9. Ballester, J. et al. Heat-related mortality in Europe during the summer of 2022. *Nat. Med.* **29**, 1857–1866 (2023).
10. Coumou, D., Di Capua, G., Vavrus, S., Wang, L. & Wang, S. The influence of Arctic amplification on mid-latitude summer circulation. *Nat. Commun.* **9**, 2959 (2018).
11. Rousi, E., Kornhuber, K., Beobide-Arsuaga, G., Luo, F. & Coumou, D. Accelerated western European heatwave trends linked to more-persistent double jets over Eurasia. *Nat. Commun.* **13**, 3851 (2022).
12. Hong, X., Lu, R. & Li, S. Amplified summer warming in Europe–West Asia and Northeast Asia after the mid-1990s. *Environ. Res. Lett.* **12**, 094007 (2017).
13. Wang, L., Xu, P., Chen, W. & Liu, Y. Interdecadal variations of the Silk Road pattern. *J. Clim.* **30**, 9915–9932 (2017).
14. Liu, Y., Sun, C. & Li, J. The boreal summer zonal wavenumber-3 trend pattern and its connection with surface enhanced warming. *J. Clim.* **35**, 833–850 (2022).
15. Bartusek, S., Kornhuber, K. & Ting, M. North American heatwave amplified by climate change-driven nonlinear interactions. *Nat. Clim. Chang.* **12**, 1143–1150 (2022).
16. Zhang, X. et al. Increased impact of heat domes on 2021-like heat extremes in North America under global warming. *Nat. Commun.* **14**, 1690 (2023).
17. Chen, Z. et al. Projected increase in summer heat-dome-like stationary waves over Northwestern North America. *npj Clim. Atmos. Sci.* **6**, 194 (2023).
18. Arblaster, J. M. & Alexander, L. V. The impact of the El Niño–Southern Oscillation on maximum temperature extremes. *Geophys. Res. Lett.* **39**, L20702 (2012).
19. Luo, M. & Lau, N.-C. Summer heat extremes in northern continents linked to developing ENSO events. *Environ. Res. Lett.* **15**, 074042 (2020).
20. Martija-Díez, M., Rodríguez-Fonseca, B. & López-Parages, J. ENSO influence on Western European summer and fall temperatures. *J. Clim.* **34**, 8013–8031 (2021).
21. Loikith, P. C. & Broccoli, A. J. The influence of recurrent modes of climate variability on the occurrence of winter and summer extreme temperatures over North America. *J. Clim.* **27**, 1600–1618 (2014).
22. Luo, M. & Lau, N.-C. Amplifying effect of ENSO on heat waves in China. *Clim. Dyn.* **52**, 3277–3289 (2019).
23. Naveena, N., Satyanarayana, G. C., Rao, K. K., Umakanth, N. & Srinivas, D. Heat wave characteristics over India during ENSO events. *J. Earth Syst. Sci.* **130**, 1–16 (2021).
24. Loughran, T. F., Pitman, A. J. & Perkins-Kirkpatrick, S. E. The El Niño–Southern Oscillation's effect on summer heatwave development mechanisms in Australia. *Clim. Dyn.* **52**, 6279–6300 (2019).
25. Reddy, P. J., Perkins-Kirkpatrick, S. E. & Sharples, J. J. Interactive influence of ENSO and IOD on contiguous heatwaves in Australia. *Environ. Res. Lett.* **17**, 014004 (2021).
26. Black, E. & Sutton, R. The influence of oceanic conditions on the hot European summer of 2003. *Clim. Dyn.* **28**, 53–66 (2007).
27. Duchez, A. et al. Drivers of exceptionally cold North Atlantic Ocean temperatures and their link to the 2015 European heat wave. *Environ. Res. Lett.* **11**, 074004–074010 (2016).
28. McKinnon, K. A., Rhines, A., Tingley, M. P. & Huybers, P. Long-lead predictions of eastern United States hot days from Pacific sea surface temperatures. *Nat. Geosci.* **9**, 389–394 (2016).
29. Seneviratne, S. I. et al. Investigating soil moisture–climate interactions in a changing climate: a review. *Earth Sci. Rev.* **99**, 125–161 (2010).
30. Domeisen, D. I. V. et al. Prediction and projection of heatwaves. *Nat. Rev. Earth Environ.* **4**, 36–50 (2023).
31. Miralles, D., Teuling, A. & Heerwaarden, C. Mega-heatwave temperatures due to combined soil desiccation and atmospheric heat accumulation. *Nat. Geosci.* **7**, 345–349 (2014).
32. Zhang, T. et al. An energetics tale of the 2022 mega-heatwave over central-eastern China. *npj Clim. Atmos. Sci.* **6**, 162 (2023).
33. Mueller, B. & Seneviratne, S. I. Hot days induced by precipitation deficits at the global scale. *Proc. Natl Acad. Sci. USA* **109**, 12398–12403 (2012).
34. Quesada, B., Vautard, R., Yiou, P., Hirschi, M. & Seneviratne, S. I. Asymmetric European summer heat predictability from wet and dry southern winters and springs. *Nat. Clim. Chang.* **2**, 736–741 (2012).
35. Qiao, L. et al. Soil moisture–atmosphere coupling accelerates global warming. *Nat. Commun.* **14**, 4908 (2023).
36. Vogel, M. M. et al. Regional amplification of projected changes in extreme temperatures strongly controlled by soil moisture–temperature feedbacks. *Geophys. Res. Lett.* **44**, 1511–1519 (2017).
37. Eyring, V. et al. Overview of the Coupled Model Intercomparison Project Phase 6 (CMIP6) experimental design and organization. *Geosci. Model Dev.* **9**, 1937–1958 (2016).
38. Hersbach, H. et al. The ERA5 global reanalysis. *Q. J. R. Meteorol. Soc.* **146**, 1999–2049 (2020).
39. Jia, F. et al. Enhanced North Pacific impact on El Niño/Southern Oscillation under greenhouse warming. *Nat. Clim. Chang.* **11**, 840–847 (2021).
40. Fan, H., Yang, S., Wang, C., Wu, Y. & Zhang, G. Strengthening amplitude and impact of the Pacific Meridional Mode on ENSO in the warming climate depicted by CMIP6 models. *J. Clim.* **35**, 5195–5213 (2022).
41. Ding, R. et al. Linking the North American dipole to the Pacific meridional mode. *J. Geophys. Res. Atmos.* **124**, 3020–3034 (2019).
42. Cai, W. et al. Increasing frequency of extreme El Niño events due to greenhouse warming. *Nat. Clim. Chang.* **4**, 111–116 (2014).
43. Cai, W. et al. Changing El Niño–Southern Oscillation in a warming climate. *Nat. Rev. Earth Environ.* **2**, 628–644 (2021).
44. Kumar, K. K., Rajagopalan, B. & Cane, M. A. On the weakening relationship between the Indian monsoon and ENSO. *Science* **284**, 2156–2159 (1999).
45. Fischer, E., Seneviratne, S., Vidale, P., Lüthi, D. & Schär, C. Soil moisture: atmosphere interactions during the 2003 European summer heat wave. *J. Clim.* **20**, 5081–5099 (2007).
46. Haarsma, R. J., Selten, F., Hurk, B., Hazeleger, W. & Wang, X. Drier Mediterranean soils due to greenhouse warming bring easterly winds over summertime central Europe. *Geophys. Res. Lett*. **36**, L04705 (2009).
47. Zampieri, M. et al. Hot European summers and the role of soil moisture in the propagation of Mediterranean drought. *J. Clim.* **22**, 4747–4758 (2009).
48. Orth, R., Dutra, E. & Pappenberger, F. Improving weather predictability by including land surface model parameter uncertainty. *Mon. Weather Rev.* **144**, 1551–1569 (2016).
49. Li, X. et al. Role of atmospheric resonance and land–atmosphere feedbacks as a precursor to the June 2021 Pacific Northwest Heat Dome event. *Proc. Natl Acad. Sci. USA* **121**, e2315330121 (2024).
50. Runge, J. et al. Identifying causal gateways and mediators in complex spatio-temporal systems. *Nat. Commun.* **6**, 8502 (2015).
51. Lesk, C. et al. Compound heat and moisture extreme impacts on global crop yields under climate change. *Nat. Rev. Earth Environ.* **3**, 872–889 (2022).
52. Wang, J. et al. Anthropogenically-driven increases in the risks of summertime compound hot extremes. *Nat. Commun.* **11**, 528 (2020).

53. Wang, J. et al. Anthropogenic emissions and urbanization increase risk of compound hot extremes in cities. *Nat. Clim. Chang.* **11**, 1084–1089 (2021).
54. Zhang, K. et al. Increased heat risk in wet climate induced by urban humid heat. *Nature* **617**, 738–742 (2023).
55. Raymond, C., Matthews, T. & Horton, R. M. The emergence of heat and humidity too severe for human tolerance. *Sci. Adv.* **6**, eaaw1838 (2020).
56. Fischer, E. M. & Schär, C. Consistent geographical patterns of changes in high-impact European heatwaves. *Nat. Geosci.* **3**, 398–403 (2010).
57. Perkins, S. E. & Alexander, L. V. On the measurement of heat waves. *J. Clim.* **26**, 4500–4517 (2013).
58. Amaya, D. J. The Pacific meridional mode and ENSO: a review. *Curr. Clim. Chang. Rep.* **5**, 296–307 (2019).

Acknowledgements

S.Y. and T.Z. are supported by the National Natural Science Foundation of China (Grant 42088101, 42275020), the Innovation Group Project of Southern Marine Science and Engineering Guangdong Laboratory (Zhuhai) (311021001), and the Guangdong Province Key Laboratory for Climate Change and Natural Disaster Studies (2020B1212060025). F.C. and C.L. are supported by the China Scholarship Council (CSC) scholarship.

Author contributions

T.Z. conceived and designed the study. F.C. conducted the analysis and drafted the manuscript. C.L., D.G., T.Z., S.Y., and J.K. provided comments and revised the manuscript. F.C., T.Z., C.L., D.G, S.Y., S.L., and J.K. discussed the scientific interpretation of the results.

Competing interests

The authors declare no competing interests.

Additional information

Supplementary information The online version contains supplementary material available at https://doi.org/10.1038/s41612-024-00779-y.

Correspondence and requests for materials should be addressed to Tuantuan Zhang.